ELSEVIER

NeuroImage

www.elsevier.com/locate/ynimg
NeuroImage 22 (2004) 1046–1059

In vivo detection of neuroarchitecture in the rodent brain using manganese-enhanced MRI

Ichio Aoki,[a] Yi-Jen Lin Wu,[b] Afonso C. Silva,[a] Ronald M. Lynch,[a] and Alan P. Koretsky[a,*]

[a] *Laboratory of Functional and Molecular Imaging, National Institute of Neurological Disorders and Stroke, National Institutes of Health, Bethesda, MD 20892-1065, USA*
[b] *Pittsburgh NMR Center for Biomedical Research, Carnegie Mellon University, Pittsburgh, PA 15213, USA*

Received 26 September 2003; revised 16 March 2004; accepted 18 March 2004

Visualizing brain anatomy in vivo could provide insight into normal and pathophysiology. Here it is demonstrated that neuroarchitecture can be detected in the rodent brain using MRI after systemic $MnCl_2$. Administration of $MnCl_2$ leads to rapid T_1 enhancement in the choroid plexus and circumventricular organs, which spreads to the CSF space in ventricles and periventricular tissue. After 1 day, there was MRI enhancement throughout the brain with high intensity in the pituitary, olfactory bulb, cortex, basal forebrain, hippocampus, basal ganglia, hypothalamus, amygdala, and cerebellum. Contrast obtained enabled visualization of specific features of neuroarchitecture. The arrowhead structure of the dentate gyrus as well as the CA1–CA3 region of the hippocampus and layers in cortex, cerebellum, as well as the olfactory bulb could be readily observed. Preliminary assignments of olfactory bulb layers, cortical layers in frontal and somatosensory cortex, and cerebellum were made. Systemic $MnCl_2$ leads to MRI visualization of neuroarchitecture nondestructively.

Keywords: Brain cytoarchitecture; Cortical layers; Molecular imaging; Choroid plexus

Introduction

Magnetic resonance imaging (MRI) is an important technique for understanding brain anatomy and function under normal and pathological conditions in vivo. A frontier for MRI is to develop approaches to obtain brain cytoarchitectural information noninvasively at a resolution high enough to determine fine structure. One promising approach is to use the sensitivity of MRI to myelin to detect gray matter myeloarchitecture. Results from in vitro fixed tissue and the brain in vivo have demonstrated that MRI-based myeloarchitecture has potential to define regional boundaries in the cortex in individuals (Barbier et al., 2002; Walters et al., 2003). Another approach is to use functional MRI techniques to define regions of the cortex. Results detecting functional MRI signal changes that reflect different regions of the visual (Kwong et al., 1992; Ogawa et al., 1992) and motor cortex (Bandettini et al., 1992), ocular dominance columns (Menon et al., 1997), ocular orientation columns (Duong et al., 2001), rodent whisker barrels (Yang et al., 1996), rodent olfactory glomeruli (Kida et al., 2002), and cortical layers (Silva and Koretsky, 2002) show much promise. A third approach is to develop molecular imaging agents that alter MRI contrast to give information about neuroarchitecture.

In his landmark paper describing MRI, Lauterbur already appreciated the usefulness of paramagnetic ions for altering contrast (Lauterbur, 1973). In this seminal work, manganese sulfate was used to alter image intensities due to changes in T_1 relaxation time. Manganese is known to be an essential trace nutrient in all forms of life. In particular, for brain function, it is a cofactor for manganese superoxide dismutase and glutamine synthetase (Carl et al., 1993; Sugaya et al., 1997). Nevertheless, the general use of manganese ion (Mn^{2+}) as an MRI contrast agent was hampered by its significant toxicity in humans (Archibald and Tyree, 1987; Aschner and Aschner, 1991; Barbeau, 1984; Donaldson, 1987; Graham, 1984). Such interest has been recently renewed, however, due to the unique biological properties of Mn^{2+}. Recent work has relied on the fact that Mn^{2+} can enter cells via voltage-gated calcium channels to enhance excitable cells in the brain (Aoki et al., 2002b; Duong et al., 2000; Lin and Koretsky, 1997) and to monitor changes in ionotropic status in the heart (Hu et al., 2001). The fact that Mn^{2+} can enter properly functioning cells has led to work aimed at developing Mn^{2+} as a cell viability indicator for cardiac applications (Brurok et al., 1999; Wendland et al., 2002). Mn^{2+} can also move along appropriate neuronal pathways and this property has been used to develop Mn^{2+} as a useful MRI contrast agent to trace neuronal pathways (Pautler et al., 1998; Saleem et al., 2002; Van der Linden et al., 2002; Watanabe et al., 2001). Using the ability of Mn^{2+} to accumulate in active cells, combined with its ability to trace neuronal pathways, has enabled mapping of areas of the olfactory bulb (OB) that respond to specific odors (Pautler and Koretsky, 2002). All of this work indicates that Mn^{2+} will be a useful molecular imaging agent to visualize functional neuroarchitecture.

There have been numerous MRI studies on the distribution and relaxation properties of Mn^{2+} in animals after the systemic admin-

* Corresponding author. Laboratory of Functional and Molecular Imaging, National Institute of Neurological Disorders and Stroke, National Institutes of Health, 10 Center Drive, 10/B1D118, Bethesda, MD, 20892-1065. Fax: +1-301-480-2558.
E-mail address: KoretskyA@ninds.nih.gov (A.P. Koretsky).
Available online on ScienceDirect (www.sciencedirect.com.)

1053-8119/$ - see front matter © 2004 Elsevier Inc. All rights reserved.
doi:10.1016/j.neuroimage.2004.03.031

istration of Mn^{2+}. Indeed, because high-level exposure to Mn^{2+} is a known basal ganglia neurotoxin, MRI has been used to follow the distribution of Mn^{2+} in the brain (Koenig et al., 1985; London et al., 1989; Newland et al., 1989; Plowchalk et al., 1987; Wan et al., 1991, 1992). When chronically exposed to high levels of Mn^{2+}, symptoms of "manganism" resembling clinical disorders collectively described as extrapyramidal motor system dysfunction develop (Archibald and Tyree, 1987; Aschner and Aschner, 1991; Barbeau, 1984; Donaldson, 1987; Gorell et al., 1997; Graham, 1984). Areas in the brain that exhibit high accumulation of Mn^{2+} after chronic exposure are mainly in the basal ganglia or striatum, the associative areas for motor functions (Heimer et al., 1995), such as ventral pallidum (VP), globus pallidus (GP), and substantia nigra (SN). Previous work has shown that on a short time scale (within a few hours), acute intraperitoneal or intracerebral administration of Mn^{2+} showed T_1 enhanced MRI signal in ventricles, especially the inner cellular layers of the ventricular luminal wall of the rat brain (London et al., 1989; Wan et al., 1991, 1992). When Mn^{2+} was administered intravenous (IV) or through inhalation, signal enhancement in T_1-weighted MRI was found in GP, putamen, caudate, and cortical gray matter in the monkey brain when studied between 5 and 300 days (Newland et al., 1989).

Due to the fact that systemic administration of Mn^{2+} leads to MRI enhancement in specific areas of the brain, it seems possible that Mn^{2+} might be useful as a brain contrast agent to define neuroarchitecture (Lin, 1997; Natt et al., 2002; Watanabe et al., 2002). Moreover, recent improvements in MRI signal-to-noise make it likely that useful MRI contrast can be obtained at doses below those that cause neurological effects. The goal of this study was to test whether neuronal architecture in the rodent brain could be measured using high-spatial resolution T_1-weighted MRI after IV administration of manganese chloride ($MnCl_2$) solution. The results indicate that a systemic administration of $MnCl_2$ leads to excellent MRI contrast in the living rodent brain to visualize many aspects of neuronal architecture. Preliminary versions of this work have been presented previously (Aoki et al., 2002a; Lin, 1997).

Materials and methods

The manganese-enhanced MRI procedure consisted of three steps: (1) systemic $MnCl_2$ administration; (2) keeping the animal for 0–14 days; (3) T_1-weighted MRI measurements. All animal work was done following the guidelines of the Animal Care and Use Committee and the Animal Health and Care Section of the National Institute of Neurological Disorders and Stroke, National Institutes of Heath (Bethesda, MD). Twenty-eight male Sprague–Dawley rats [140–170 g, Tac:N (SD), Taconic, NY] were used. For visualization of cortical layers, four groups of rats were used including normal control for cortex ($n = 3$), normal control for OB ($n = 3$), and 4 days after $MnCl_2$ administration for cortical imaging ($n = 5$) and for OB imaging ($n = 3$) after $MnCl_2$. For manganese uptake observation, four groups of rats were used for each time point, including 0–2 h ($n = 5$), 1 day ($n = 3$), 4 days ($n = 3$), and 2 weeks ($n = 3$) after $MnCl_2$ administration.

Manganese administration

For studies that imaged rats 1 day, 4 days, and 14 days after $MnCl_2$ administration, 884.3 μmol/kg $MnCl_2$ ($MnCl_2$–$4H_2O$, Sigma, St. Louis, MO) was given by infusing 2.0 ml of a 64 mM $MnCl_2$ solution at a rate of 1.8 ml/h through the tail vein. Rats were initially anesthetized with 4.0% isoflurane (Abbott Laboratories, Illinois), and then kept anesthetized with 1.5–2.0% isoflurane mixed with a 1:1:1 O_2/N_2/room air gas mixture using a facemask. During $MnCl_2$ infusion, the anesthesia was kept light between 0.5% and 1.2%. Rectal temperature was maintained at approximately 37.5 °C using warm water circulation during infusion. Glycopyrrolate (0.01 mg/kg, Robinul, A. H. Robins Company, Virginia) was injected intramuscularly for preanesthetic medication before the $MnCl_2$ infusion. After the $MnCl_2$ administration, anesthesia was discontinued and the rats were observed for up to 6 h following the end of the infusion. To avoid dehydration, saline (6.7 ml/100g) was injected subcutaneously two times, immediately and 6 h after the $MnCl_2$ infusion. The animals were kept in an incubator (30–32 °C, Thoren 96, cage-ventilated rack with temperature-controlled shelves, Thoren Caging Systems, Inc., Pennsylvania) for 24 h to maintain body temperature. For the 4- and 14-day groups, rats were moved into normal cages 24 h after the infusion. Rats woke up from the $MnCl_2$ infusion demonstrating a lethargic behavior that gradually improved over the period of 24 h following $MnCl_2$ administration. After 24 h, the behavior of the rats was normal as assessed by NIH/NINDS/AHCS Animal Health Assessment Test. For acute studies (0–2 h), the same dose of $MnCl_2$ solution was infused into the femoral or tail vein during MRI measurements. No differences between tail vein and femoral vein administration were detected (data not shown).

Animal preparation for MRI

Rats were initially anesthetized with 4.0% isoflurane, orally intubated, and then ventilated with 1.0–1.5% isoflurane and 1:1:1 O_2/N_2/room air gas mixture using a rodent ventilator (SAR-830/P, CWE, Inc., Pennsylvania). For the 0–2-h group, polyethylene catheters (PE-50, Becton Dickinson, Maryland) were placed in the femoral artery and vein for drug administration, blood pressure monitoring, and arterial blood gas measurements. The arterial blood gas measurement was performed every 30 min. Rectal temperature was maintained at approximately 37.5 °C using a warm water blanket. Just before MRI measurements, pancuronium bromide (2.5 mg/kg, Baxter Health Care Corp., California) was injected intraperitoneally to suppress motion. In the acute infusion group (0–2 h, $n = 5$), the mean arterial blood pressure was 99.4 ± 31.1 mm Hg. Typically, arterial blood pressure was gradually decreased during manganese IV infusion. The mean arterial blood pressure between 0 and 60 min was 122.83 ± 31.1 mm Hg, and the one between 60 and 120 min was 75.9 ± 25.9 mm Hg. Blood gases and pH of rats were within normal physiological ranges: pH = 7.0–7.4, $PaCO_2$ = 30–40 mm Hg, and oxygen partial pressure (PaO_2) = 90–110 mm Hg.

MRI measurements

Proton MRI was performed in an 11.7-T, 31-cm bore magnet (Magnex Scientific Ltd., U.K.) interfaced to a Bruker Avance console (Bruker Medical GmbH, Germany). A 35-mm-diameter birdcage coil (Bruker Medical GmbH) was used for whole brain coverage and a 10-mm-diameter surface coil (made in house) was used for higher signal to noise over the OB and cortex. For two rats in the cortical imaging group, combination of a 90-mm-diameter birdcage transmitter coil (made in house) and a 15-mm-diameter receiving surface coil (made in house) was used to improve RF homogeneity and sensitivity.

For whole brain studies of manganese uptake, T_1-weighted multislice two dimensional (2D) spin echo (SE) images were obtained. The MRI acquisitions for 2D imaging were performed with the following parameters; repetition time (TR)/echo time (TE) = 300/10.5 ms, matrix size = 256 × 256, field of view (FOV) = 25.6 × 25.6 mm, slice thickness (ST) = 1 mm, number of averages (NA) = 8. Slice orientation was coronal (10 slices with and without 1-mm slice offset), horizontal (5 slices with and without 1-mm slice offset), and sagittal (5 slices). For these images, the nominal voxel resolution was 100 × 100 × 1000 μm. In some cases, three-dimensional (3D) imaging were performed with the following parameters: 3D SE sequence; TR/TE = 250/7.3 ms; matrix size = 256 × 256 × 128; FOV = 19.2 × 19.2 × 9.6 mm; and NA = 2. The total acquisition time was 273 min. On some images (see figure captions), T_1-weighted images were acquired with inversion recovery rather than using a short TR. For inversion recovery, parameters were the following: inversion time = 1100 ms; TR/TE = 4000/11.2 ms; matrix size = 512 × 256; FOV = 38.4 × 19.2 mm; ST = 1 mm; and NA = 1. For the acute 0–2 h group, T_1-weighted MRI sets for control were obtained using the same parameters before $MnCl_2$ administration. After that, sequential scanning was beginning after starting $MnCl_2$ infusion. Two sets of T_1-weighted multislice MRI acquisitions, consisting of coronal and horizontal planes, were repeated 12 times. The acquisitions of sequential scanning were performed with the following parameters: conventional 2D SE sequence; TR/TE = 300/10.5 ms; matrix size = 256 × 256; FOV = 25.6 × 25.6 mm; ST = 1 mm; NA = 4; and imaging plane = coronal (10 slices) and horizontal (5 slices). One set of 2D images took 10 min so that 12 sets could be acquired over 2 h.

For higher resolution to exam layers in the OB and cortex, three sets of T_1-weighted multislice 2D images and one T_1-weighted 3D image were obtained per animal. The MRI acquisitions for 2D imaging were performed with the following parameters: conventional 2D SE sequence; TR/TE = 300/10.5 ms; matrix size = 256 × 256; FOV = 12.8 × 12.8 mm; ST = 0.75 mm; NA = 12, and imaging plane = coronal (8 slices), horizontal (4 slices), and sagittal (5 slices). Thus, the nominal voxel resolution was 50 × 50 × 750 μm for 2D imaging. The MRI acquisitions for 3D imaging were performed with the following parameters: 3D SE sequence; TR/TE = 300/11.3 ms; matrix size = 256 × 128 × 64; FOV = 15.4 × 7.7 × 3.8 mm; NA = 6. The total acquisition time was 250 min to achieve a nominal resolution of 60 μm.

Image reconstruction and analysis were performed using ParaVision (Bruker Medical GmbH), MRVision (Ver. 1.5, MRVision Co., Massachusetts), and NIH Image (Ver. 1.62, NIH, Maryland). Equivalent brain slices were placed side by side for direct comparison. All analyses were performed on a Linux-PC (Linux Mandrake 7.0, Mandrake Soft Inc., California) and Macintosh (MacOS 9.2 and 10.2, Apple Computer Inc., California). Data are presented as mean ± standard deviation (SD) normalized to the background noise from each animal. Statistical significance was set to $P < 0.05$. For statistical comparison of cortical layers, regions of interest (ROI) were defined as mitral cell layer and granular cell layer in the OB based on the rat brain atlas (Paxinos and Watson, 1998). In addition, ROIs were also defined as cortical layers from 1 to 5 based on the atlas of rat forebrain (Paxinos et al., 1999). Twenty pixels were sampled from each of the ROIs. Multiple comparison post hoc tests (Bonferroni–Dunn method) were used for comparison of signal intensities. Statistical calculations were performed using StatView (Ver. 5.0, SAS Institute, Inc., North Carolina).

Results

$MnCl_2$ infusion leads to MRI signal enhancement in the rodent brain

Fig. 1 shows three slices from T_1-weighted MRI of a control rat (Figs. 1A) and a rat 1 day after IV infusion of $MnCl_2$ solution

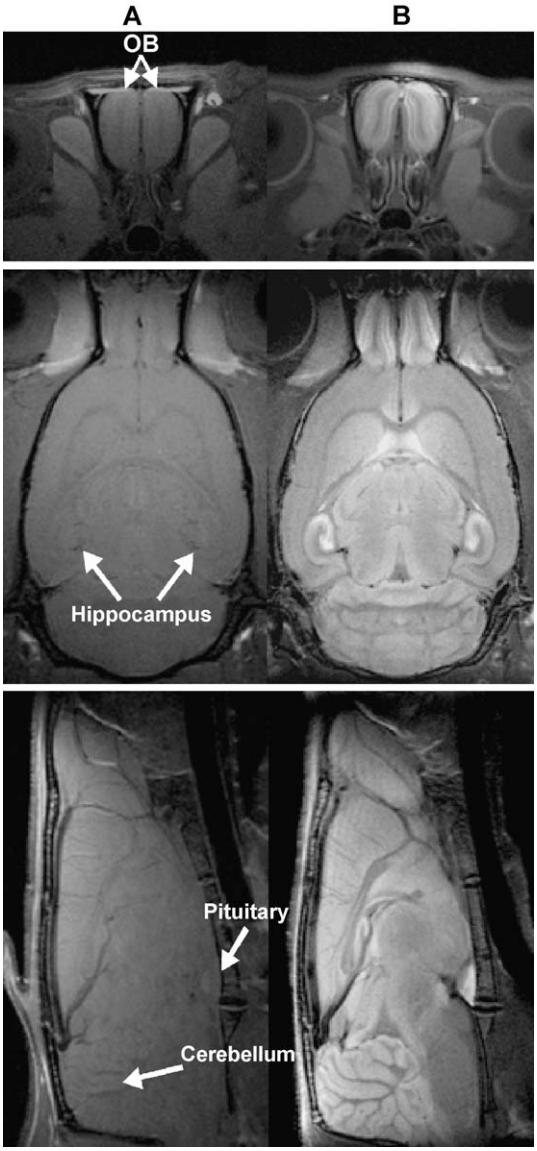

Fig. 1. T_1-weighted MRI after systemic $MnCl_2$ administration in the rat. T_1-weighted MRI of a control rat (column A) and a rat 1 day after IV infusion of $MnCl_2$ solution (column B). Top row shows transverse slices at the level of the olfactory bulb (OB, Bregma: +7 mm). The middle row shows horizontal slices including the hippocampal formation (Bregma: −6 mm). The bottom row shows sagittal slices. The signal intensity of the T_1-weighted MRI was enhanced prominently 1 day after systemic administration of $MnCl_2$ in the rat. There were characteristic signal enhancements that were large in the olfactory bulb (OB), hippocampus, cerebellum, and pituitary.

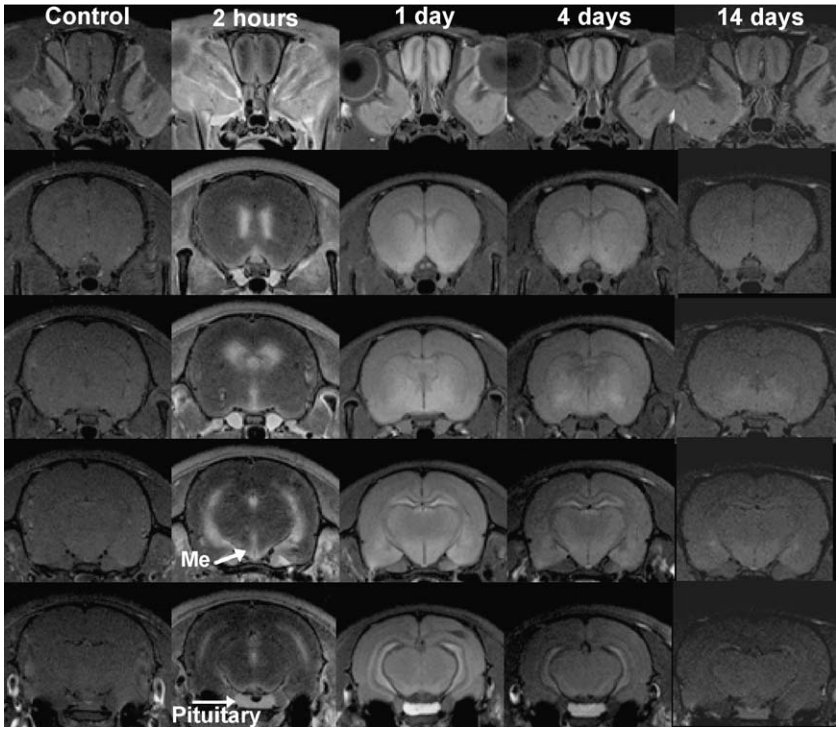

Fig. 2. T_1-weighted MRI reflecting manganese distribution in a rat brain over a 2-week period following systemic IV $MnCl_2$ administration. MRI was performed on separate animals before (Control), 2 h, 1 day, 4 days, and 14 days after the administration of $MnCl_2$. The top, second, third, fourth, and bottom line shows transverse slices at the level of the olfactory bulb, Bregma +2, 0, −2, and −4 mm, respectively. Controls that had not received $MnCl_2$ showed very little contrast and low signal. Within 2 h of infusion of $MnCl_2$, there was large enhancement in the regions with large ventricular space and circumventricular organs such as pituitary (Pit), pineal gland, and median eminence (Me). By 1 day, the enhancement had spread throughout the brain but showed a heterogeneous, yet typical enhancement. The olfactory bulbs, hippocampus, and deep brain structures showed the largest enhancement. By 1 day, the large enhancements in the ventricles detected after 2 h were reduced to pre-$MnCl_2$ infusion levels. After 1 day, there were no large changes in the distribution of enhancement. Enhancement was clearly visible at 4 days but declined steadily to near-control levels by 14 days.

(Figs. 1B). The signal intensity of the T_1-weighted MRI was enhanced 1 day after systemic administration of $MnCl_2$ in the rat. There were characteristic signal enhancements that were large in the OB, hippocampus (CA), basal forebrain, cerebellum, and pituitary (Pit). Signal was also increased throughout the entire brain but to a smaller extent than the structures that showed the largest enhancement. A similar pattern of enhancement was detected in the rat brain.

Time course of brain MRI enhancement

Fig. 2 shows the distribution of $MnCl_2$ in rat brain following systemic IV $MnCl_2$ administration over a 2-week time period. MRI was performed on separate animals before, 2 h, 1 day, 4 days, and 14 days after the administration of $MnCl_2$. Controls that had not received $MnCl_2$ showed very little contrast and low signal in these T_1-weighted images. Quantitative data summarizing signal changes in several brain areas is summarized in Table 1. Within 2 h of infusion of $MnCl_2$, there was large enhancement in the regions with large ventricular space and circumventricular organs such as Pit, pineal gland (Pi), and median eminence (Me) in the brain. By 1 day, the enhancement had spread through the brain but showed a heterogeneous, yet typical enhancement. The OBs, CA, and deep brain structures showed the largest enhancement. By 1 day, the large enhancements in the ventricles detected after 2 h were reduced to pre-$MnCl_2$ infusion levels. After 1 day, there were no large changes

Table 1
Comparison of relative signal in different regions of the rat brain after IV administration of $MnCl_2$

	Control	2 h	1 day	4 days	14 days
Olfactory bulb	8.56 ± 0.74	8.43 ± 0.97	26.97 ± 5.99[a]	16.01 ± 0.74[a]	10.62 ± 2.01
Olfactory ventricle	8.21 ± 0.67	6.83 ± 1.04	18.90 ± 4.10[a]	12.34 ± 1.07[a]	8.68 ± 1.56
Cortex	6.91 ± 0.39	6.18 ± 0.84	14.71 ± 1.90[a]	11.67 ± 0.43[a]	6.84 ± 0.77
Corpus callosum	7.35 ± 0.50	6.25 ± 0.72	15.04 ± 1.94[a]	10.93 ± 0.84[a]	6.90 ± 0.72
Caudate putamen	8.67 ± 0.42	7.30 ± 1.01	18.58 ± 2.17[a]	14.83 ± 0.83[a]	8.97 ± 1.02
Hypothalamus	8.95 ± 0.57	8.37 ± 1.01	22.22 ± 2.65[a]	18.11 ± 2.08[a]	11.10 ± 1.45
CA3	7.11 ± 0.34	7.05 ± 1.21	21.02 ± 2.47[a]	15.07 ± 2.48[a]	7.92 ± 1.80
Amygdala	8.21 ± 0.84	9.22 ± 0.63	21.42 ± 3.32[a]	15.98 ± 2.75[a]	9.48 ± 1.48
Anterior pituitary	7.63 ± 0.89	15.99 ± 1.41[a]	29.54 ± 3.93[a]	25.30 ± 5.49[a]	9.13 ± 2.64

[a] Significant difference vs. control (time-course comparison), level of significance $P < 0.005$ for Bonferroni–Dunn (significance level = 5%, $n = 3$).

in the distribution of enhancement. Enhancement was clearly visible at 4 days but declined steadily to near control levels by 14 days.

A closer examination of the hyperintensity that first appeared in the cerebrospinal fluid (CSF) compartment 2 h after infusion was undertaken by acutely administering $MnCl_2$ with the animal in the magnet. Within 5 min after starting the $MnCl_2$ infusion, the choroid plexus (CP), Pit, and Pi were the first brain structures to be enhanced. Fig. 3A shows an expanded horizontal view of the left ventricle 5, 10, and 100 min after $MnCl_2$ infusion. Fig. 3B shows a T_2-weighted MRI obtained before infusion of $MnCl_2$, indicating the distribution of CSF. Fig. 3C shows this region reproduced from the Paxinos rat brain atlas (Paxinos and Watson, 1998). Enhancement first occurred highly localized in the ventricle corresponding

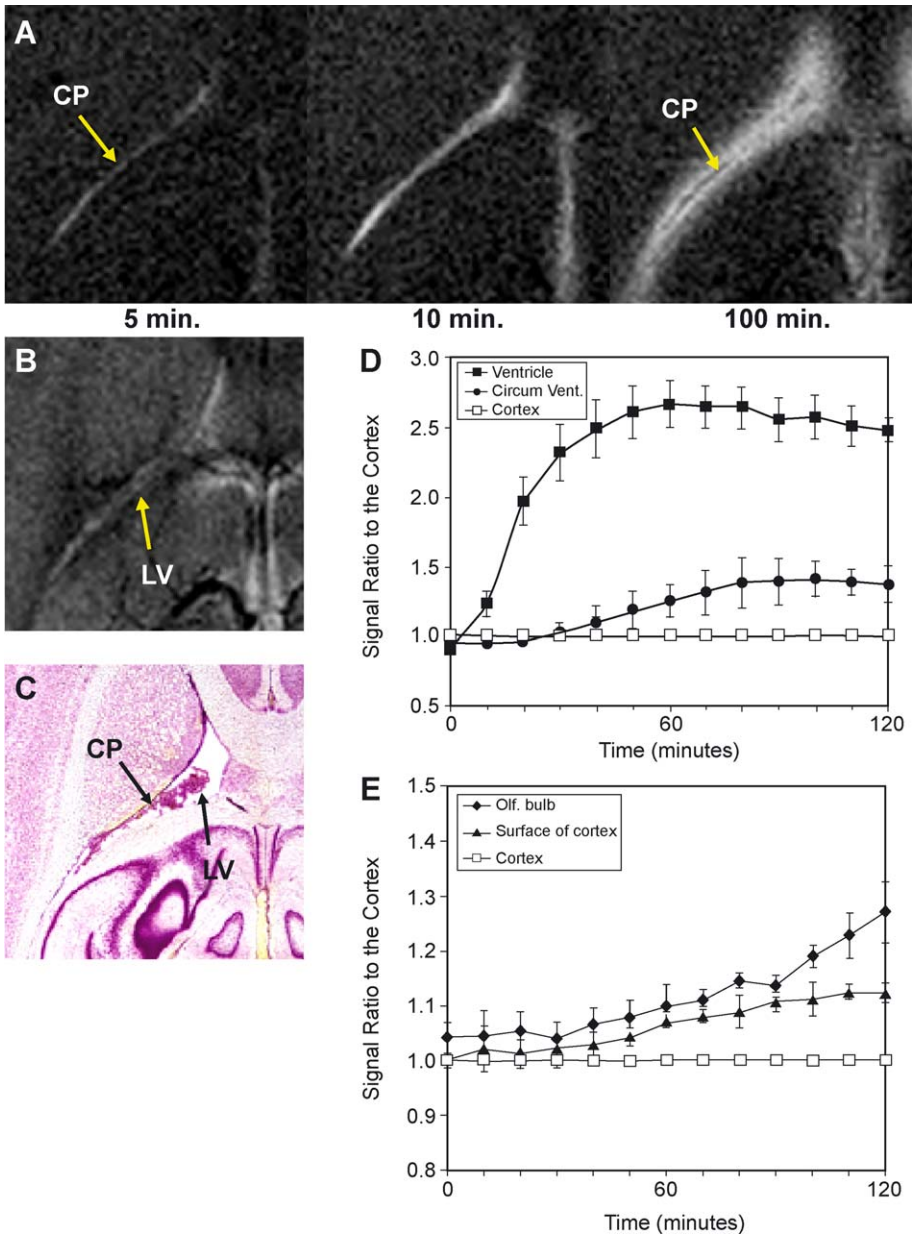

Fig. 3. Dynamic imaging of manganese uptake via the choroid plexus. An expanded horizontal view of the left ventricle: (A) Sequential T_1-weighted MRI taken at 5, 10, and 100 min after $MnCl_2$ infusion. (B) T_2-weighted MRI obtained before infusion of $MnCl_2$, indicating the distribution of CSF, and (C) histology of this region from the Paxinos rat brain atlas. Enhancement first occurred highly localized in the lateral ventricle (LV) corresponding to the distribution of choroid plexus (CP) (A, left). By 10 min, the enhancement diffused to fill up the entire CSF space in the ventricle (A, middle). After stopping the infusion and 100 min after first infusing $MnCl_2$, the left ventricle remained enhanced, the CP lost enhancement and was detected as a darker line within the ventricle (A, right). At 100 min after starting to infuse $MnCl_2$, the enhanced region spread into the periventricular brain tissue that touches CSF beyond the region of the left ventricle, such as the fimbria of the hippocampus, and lateral septal nucleus. Quantitative time courses of signal normalized to the cortex (open square) in the ventricle (filled square, D), periventricular tissue (filled circle, D), periphery of the olfactory bulb (filled diamond, E), and surface of the cortex (filled triangle, E) over the first 2 h after administrating $MnCl_2$ are shown in D and E. Signal increased rapidly in the ventricle reaching almost three times the intensity detected before administration of $MnCl_2$ (D). In contrast, signal intensities increased slowly for 60–120 min in the periventricular tissue, surface of cortex, and periphery of olfactory bulb (D, E).

to the distribution of CP. By 10 min, the enhancement diffused to fill up the entire CSF space in the ventricle including the subarachnoid space. After stopping the infusion and 100 min after first infusing $MnCl_2$, the left ventricle remained enhanced, the CP lost enhancement and was detected as a darker line within the ventricle. At 100 min after starting to infuse $MnCl_2$, the enhanced region spread into the periventricular brain tissue that touches CSF beyond the region of the left ventricle, such as the fimbria of hippocampus and lateral septal nucleus. This initial enhancement of CP, enhancement of CSF, and then enhancement of the periventricular tissue was observed in the third and fourth ventricle as well as the left ventricle. Figs. 3D,E show time courses of signal normalized to the cortex in the ventricle, periventricular tissue, periphery of the OB, and surface of the cortex over the first 2 h after administrating $MnCl_2$. Signal increased rapidly in the ventricle reaching almost three times the intensity detected before administration of $MnCl_2$. In contrast, signal intensities were increased slowly for 60–120 min in the periventricular tissue, surface of cortex, and periphery of OB. In the deeper areas of cortex and some deeper brain structures, there was minimal signal enhancement after 2 h (Table 1).

Summary of manganese-dependent enhancement in the rodent brain

Below is a description of different regions of the brain and how they were affected by $MnCl_2$ infusion. Brain area assignments follow Paxinos and Watson (Paxinos and Watson, 1998; Paxinos et al., 1999) by correlation.

Ventricle, circumventricular organs, and CSF: Within 2 h after the Mn^{2+} infusion the lateral ventricle, third, fourth ventricles (first CP and then CSF), and interventricular foramen and aqueduct such as Sylvius showed enhanced signal. The subarachnoid space around the whole brain also enhanced within 10 min of administering $MnCl_2$, especially around the OB. In addition to ventricles, the signal intensity of the CP and circumventricular organs that have no blood–brain barrier (BBB) such as Pit, Pi, Me, and subfornical organ also increased rapidly after administration of $MnCl_2$. It was observed that signal surrounding the area postrema and the vascular organ of the lamina terminals was also increased. By 1 day, the enhancement in the ventricles (CSF and CP) had returned to near control levels. Most of the circumventricular organs remained enhanced and enhancement decreased on a similar time course over the 1-day to 2-week time scale as the rest of the brain (Fig. 2).

Olfactory bulb: The OB was one of the brain structures with the greatest enhancement. Within 10 min of infusion of $MnCl_2$, enhancement occurred in the subarachnoid space and the olfactory nerve. By 120 min after infusing $MnCl_2$, the enhanced region was spread into most of the OB, especially in the outer surface such as olfactory nerve layer and glomerular layer (Fig. 2). At 1 day, enhancement increased in the glomerular layer and the mitral cell layer and then decreased slowly over the next 2 weeks (Fig. 2).

Hippocampus: The CA, like the OB, also showed very high signal enhancement 1 day after administration of $MnCl_2$ in the rat (Fig. 1B, middle panel). There was no early enhancement of the CA up to 2 h after administration of $MnCl_2$.

Cortical areas: All cortical areas had increased intensity compared to controls at 1 day after administration of $MnCl_2$, which decreased slowly over 2 weeks. There was little contrast in cortical areas at 2 h after $MnCl_2$ administration. In general, the extent of cortical enhancement was lower as compared to the CA, OB, and cerebellum. Signal enhancement in cortical gray matter was identified by the increased relative contrast between the gray matter and the corpus callossum compared to controls. The cortical areas ventral to the rhinal fissure such as the amygdala and pyriform cortex were enhanced more than other cortical areas and almost as much as CA.

Subcortical areas: Subcortical areas that lay at the ventral end of the brain were also enhanced at 1 day after $MnCl_2$ administration. The degree of enhancement was intermediate between that found in the CA and OB and that found in most of the cortex. The ventral subcortical area of the brain contains many nuclei that are difficult to separate by cytoarchitecture, so it is usually called the basal forebrain. The areas that had high signal intensity were the Pit, SN, hypothalamus, GP, VP, olfactory tubercle, shell of nucleus accumbens (AcbSh, AcbC), and olfactory nuclei (AOD, AOE). The majority of these areas belong to the ventral part of

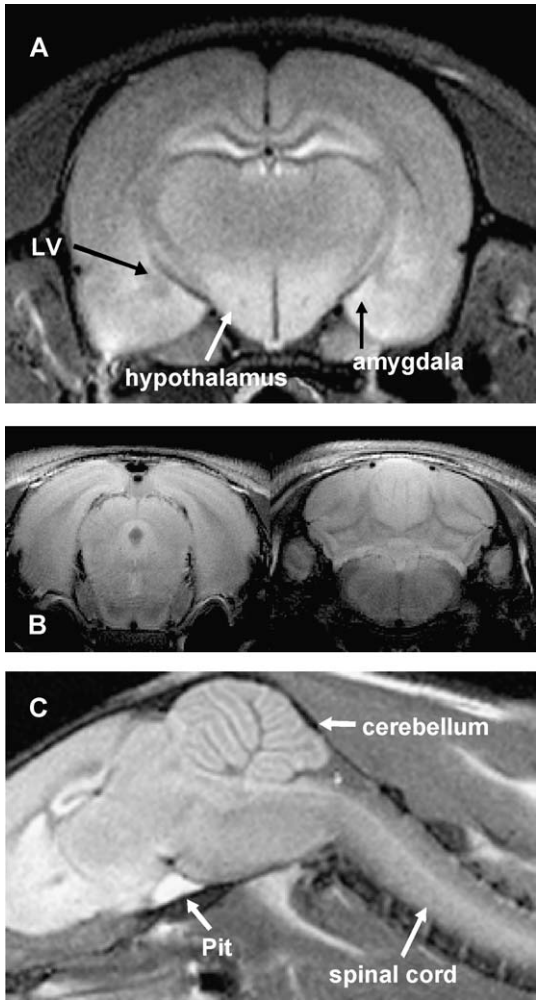

Fig. 4. T_1-weighted MRI of brainstem in rat after systemic $MnCl_2$ administration. T_1-weighted MRI from the brain stem, cerebellum, and spinal cord in rat brain 1 day after systemic IV $MnCl_2$ administration. There was significant signal enhancement in the brain stem (A, B) and spinal cord (C) 1 day after $MnCl_2$ administration. Amygdala and hypothalamus were enhanced in the occipital brain. Cerebellum also showed large enhancement 1 day after $MnCl_2$ administration. The enhancement detected after 1 day was heterogeneous, followed sulci in cerebella cortex, and correlated with the cell dense molecular and granule cell layers.

the basal ganglia or the ventral striatum, especially the ventral striatopallidal system (Heimer et al., 1995). We include SN; although it is part of the brain stem, it is usually classified as part of striatum by its function. These are the areas of the brain thought to be affected when manganese toxicity leads to Parkinsonian-like tremors.

Hypothalamic nuclei were also enhanced. However, the dorsal part of striatum such as CP, subthalamic nuclei, and the core of nucleus accumbens had less signal enhancement than the ventral striatum but still had higher intensity than cerebral cortex. Thalamic nuclei appeared less intense than the ventral striatum. Some other cerebral areas such as a part of the superior colliculus, inferior colliculus, and tegmental area also appeared enhanced in the images but the assignments of these areas are less precise because they are not as intensely enhanced and their boundaries were less well defined.

Brain stem and spinal cord: There was significant signal enhancement in the brain stem and spinal cord in the rat (Figs. 4A,B) 1 day after $MnCl_2$ administration that also appeared heterogeneous. For instance, area postrema, periaqueductal gray, and

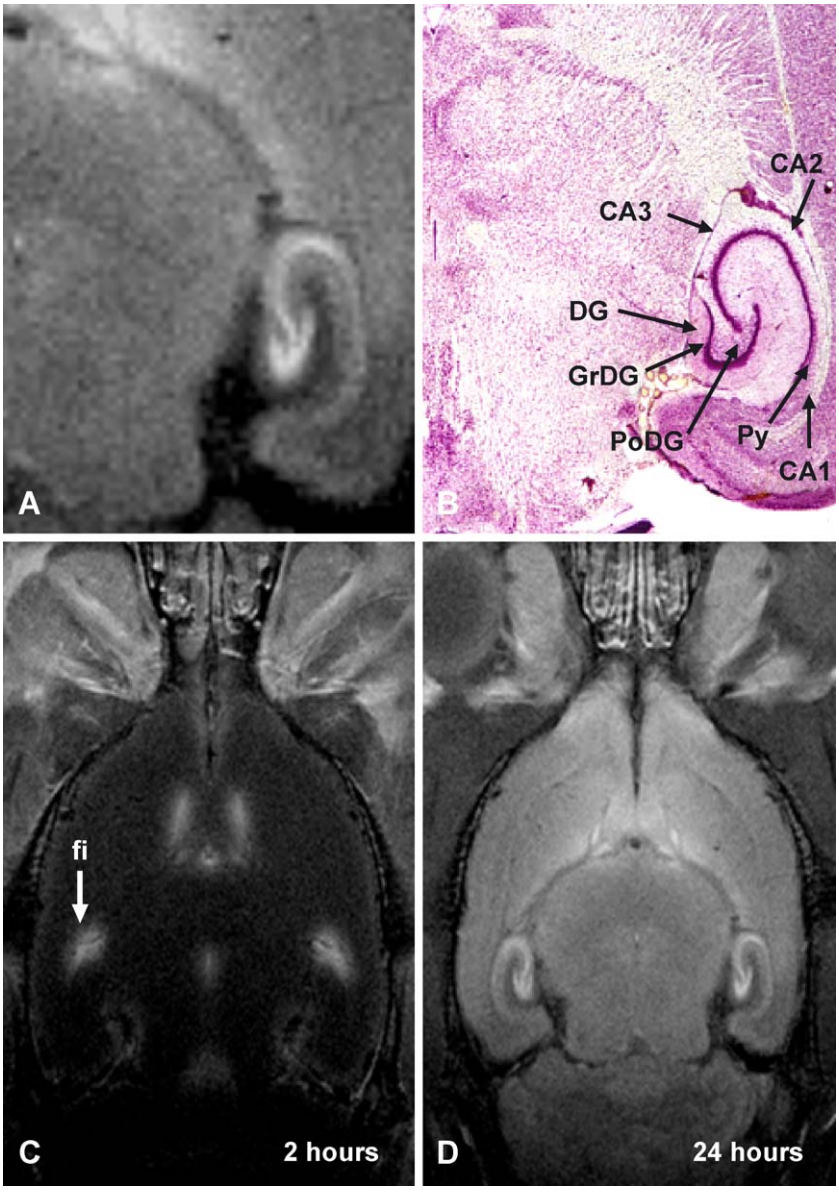

Fig. 5. T_1-weighted MRI of the hippocampal formation in the rat after systemic $MnCl_2$. Horizontal slices (Bregma: −6 mm) of T_1-weighted MRI from the hippocampus of a rat after $MnCl_2$ administration: (A) enlarged image 24 h after $MnCl_2$ infusion, (B) histology of this region from the Paxinos rat brain atlas, and T_1-weighted MRI, (C) 2 h, and (D) 24 h after $MnCl_2$ administration to the same rat. The characteristic arrowhead-shaped DG and hippocampal formation are readily detected and is in excellent agreement with histology from a corresponding slice taken from the rat brain atlas. The cell dense granular (GrDG) and polymorph layers (PoDG) of the DG enhanced in comparison with surrounding tissue. In addition to DG, signal enhancement was observed in the cell dense pyramidal cell layer (Py) of the CA1–3 (Ammon's horn) region of the hippocampus. Areas of the hippocampus that correlated with DG and CA3 in the hippocampal formation have had slightly higher intensity than CA1 (A). The hippocampus was not enhanced 2 h after $MnCl_2$ administration; however, fimbria of hippocampus and periventricular tissues near the lateral ventricle were enhanced (C). The DG and Ammon's horn region of the hippocampus was enhanced more than surrounding tissue 1 day after $MnCl_2$ administration (D).

raphe nuclei enhanced in addition to visual cortex. Areas that largely correlate to pontine nuclei enhanced less, whereas areas dorsal to pontine nuclei that largely correlate to reticular nuclei appeared brighter. The gray matter of the spinal cord enhanced more than surrounding white matter.

Cerebellum: Cerebellum also showed large enhancement (Figs. 1 and 4C) 1 day after $MnCl_2$ administration. This enhancement slowly decreased over the course of 2 weeks. Signal enhancement in the cerebellum was not detected at 2 h after $MnCl_2$. The enhancement detected after 1 day was heterogeneous, followed sulci in cerebella cortex, and correlated with the cell dense molecular and granule cell layers.

White matter nerve tracks or cell bridges such as corpus callosum, cingulum, anterior commissure, and fornix appeared to have the least enhancement among all brain areas at all time points after administering $MnCl_2$.

Visualization of cytoarchitecture in the rodent brain using manganese-enhanced MRI

It would be very interesting if $MnCl_2$ enhanced regions of the brain in a selective manner to give information about cytoarchitecture in the intact animal. To address this, high-resolution MRI was performed to look at the CA, OB, and cortex.

Hippocampus: Fig. 5A shows T_1-weighted MRI from the CA of a rat 1 day after $MnCl_2$ administration. The characteristic arrowhead shaped DG area is readily detected and is in excellent agreement with histology from a corresponding slice taken from the rat brain atlas (Fig. 5B; Paxinos and Watson, 1998). The cell dense granular (GrDG) and polymorph layers (PoDG) of the DG enhanced in comparison with surrounding tissue. In addition to DG, signal enhancement was observed in the cell dense pyramidal cell layer (Py) of the Ammon's horn region of the CA. Areas of the CA that correlated with DG and CA3 in the hippocampal formation had slightly higher intensity than CA1 (Table 2A; Fig. 5A). In addition, DG had higher enhancement than CA3 (Table 2C). Figs. 5C,D show horizontal slices of T_1-weighted MRI of the same rat obtained at 2 h and 1 day, respectively. The CA was not enhanced 2 h after $MnCl_2$ administration; however, fimbria of hippocampus and periventricular tissues near the lateral ventricle were enhanced (Fig. 5C). The DG and Ammon's horn region of the CA was enhanced more than surrounding tissue 1 day after $MnCl_2$ administration (Fig. 5D).

Table 2
Comparison of relative signal in regions of the hippocampus, olfactory bulb, and cortex 24 h after systemic $MnCl_2$ administration

(A) Hippocampus

Control	$+Mn^{2+}$ CA1	$+Mn^{2+}$ CA3	$+Mn^{2+}$ DG
10.21 ± 1.63	19.67 ± 2.24[a]	25.17 ± 2.29[a,b]	24.44 ± 1.45[a]

(B) Olfactory bulb

	Mitral cell layer	Glomerular layer
Control	9.61 ± 0.60	9.62 ± 0.38
$+Mn^{2+}$	20.33 ± 1.07[c]	15.50 ± 0.89

(C) Cortical layers

Control	$+Mn^{2+}$ layer 1	$+Mn^{2+}$ layer 2	$+Mn^{2+}$ layer 3	$+Mn^{2+}$ layer 4/5	$+Mn^{2+}$ layer 6
9.66 ± 1.61	10.45 ± 1.19	14.03 ± 0.66[d,e]	11.53 ± 0.32	14.70 ± 0.36[d,e,f]	11.70 ± 0.36

[a] Significant difference ($P < 0.0001$) vs. control (average of the hippocampus).
[b] CA3 is significantly greater than CA1 ($P < 0.0083$).
[c] Significant difference vs. Mn^{2+} administrated glomerular layer, $P < 0.0001$.
[d] Significant difference ($P < 0.0001$) vs. control (average of the cortex).
[e] Significant difference ($P < 0.0033$ (layer 2) and $P < 0.0001$ (layer 4/5)) vs. layer 1.
[f] Significant difference ($P < 0.0033$) vs. layer 3 and 6.

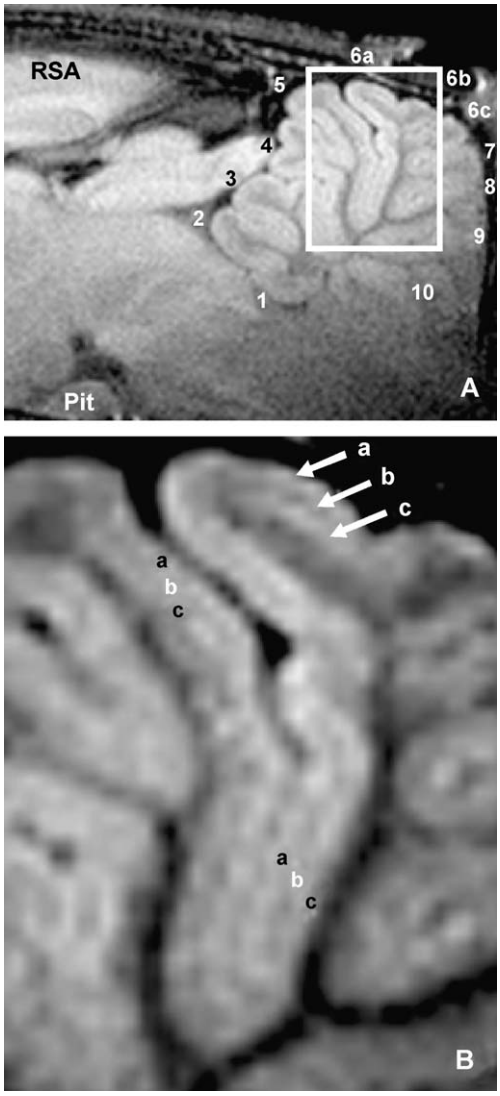

Fig. 6. Manganese-enhanced MRI of the layer structure of the cerebellum. Layer structu\re of the cerebellum detected by T_1-weighted MRI in the rat: (A) Sagittal slice of T_1-weighted MRI 4 days after administration of $MnCl_2$; (B) interpolated magnification of white square on A. The numbers show each of the cerebellar lobules. Three layers are identified as the bright molecular cell layer (a), the darker Purkinji cell layer (b), and the bright granule cell layer (c). This image was detected with an inversion recovery spin-echo sequence.

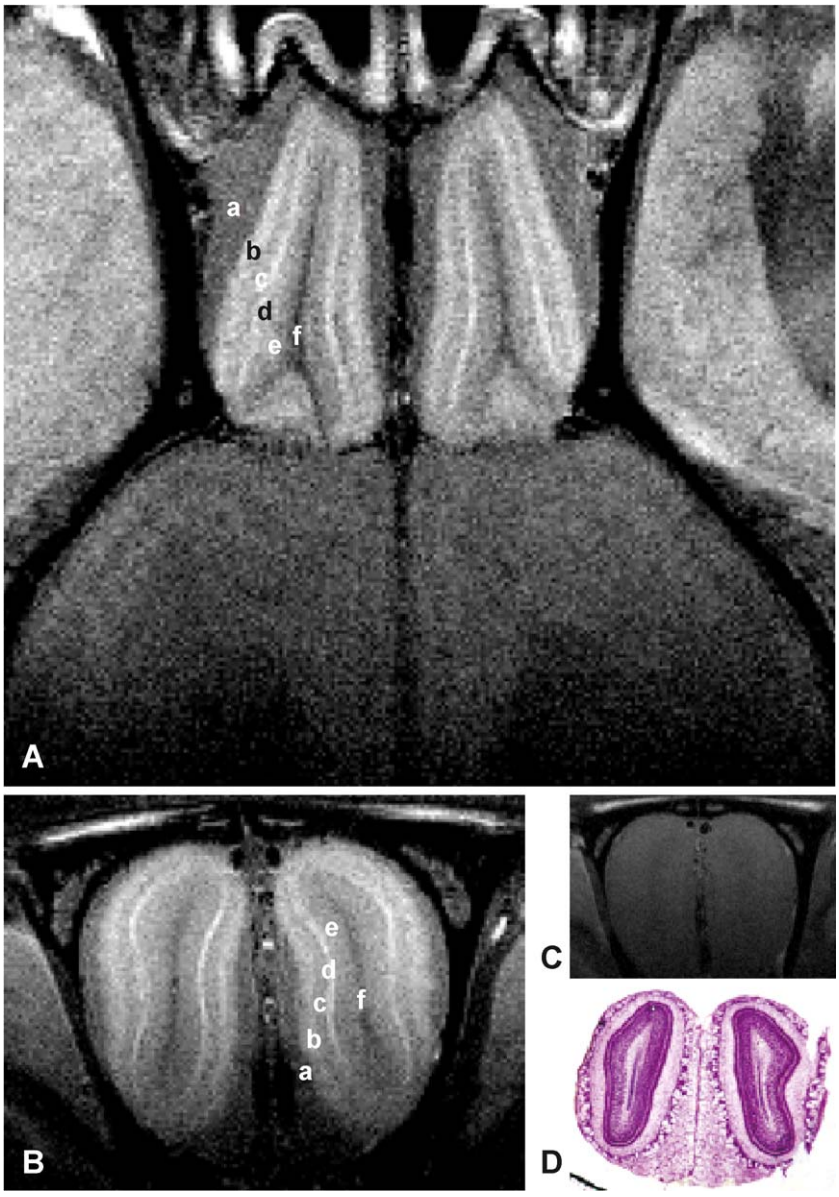

Fig. 7. Manganese-enhanced MRI of the layer structure of the olfactory bulb. Layer structure of the olfactory bulb detected by high spatial resolution (50 × 50 × 750 μm) T_1-weighted MRI 4 days after administration of $MnCl_2$: (A) horizontal and (B) coronal slices and of T_1-weighted MRI 1 day after administration of $MnCl_2$; (C) coronal slice of T_1-weighted MRI in control rat; and (D) histology of this region from the Paxinos rat brain atlas. Controls that had not received $MnCl_2$ (C) showed very little contrast and low signal. Different layers of the bulb are readily apparent and can be assigned when compared to a histological section (D). Six distinct layers of MRI signal can be detected, which are labeled a–f (B); (a) olfactory nerve layer, (b) glomerular layer, (c) external plexiform layer, (d) mitral cell layer, (e) encompasses the internal plexiform layer, granule cell layer and ependymal layer, and (f) olfactory ventricle.

Cerebellum: Fig. 6A demonstrates that the layer structure of the cerebellum was enhanced using inversion recovery MRI. All of cerebellar lobules from first to tenth were dramatically enhanced. On the other hand, white matter and fissures such as primary fissure, preculminate fissure, and prepyramidal fissure were enhanced less. Fig. 6B shows an interpolated magnification of the 5th and 6a cerebellar lobules on the same rat. Three layers are identified as the bright molecular cell layer (Fig. 6B, a), the dark Purkinji cell layer (Fig. 6B, b), and the bright granule cell layer (Fig. 6B, c).

Olfactory bulb: Figs. 7A,B demonstrate that the layer structure of the OB was readily detected 1 day after administration of $MnCl_2$. For comparison, a control that had not received $MnCl_2$ is shown in Fig. 7C. Different layers of the bulb are readily apparent and can be assigned when compared to a comparable histological section (Fig. 7D; Paxinos and Watson, 1998). Six distinct layers of MRI signal can be detected, which are labeled a–f in Fig. 7B. There are eight layers in the bulb. The MRI detected layers were assigned comparing to the atlas histology and are (from the outside in); a, olfactory nerve layer; b, glomerular layer; c, external plexiform layer; d, mitral cell layer; e, encompasses the internal plexiform layer, granule cell layer and ependymal layer; f, olfactory ventricle. All layers are readily detected except there is no distinction between the inner, low cell density layers consisting of the internal plexiform layer, granule cell layer, and ependymal layer. Table 2B shows that the relative signal from the glomerular layer and mitral cell

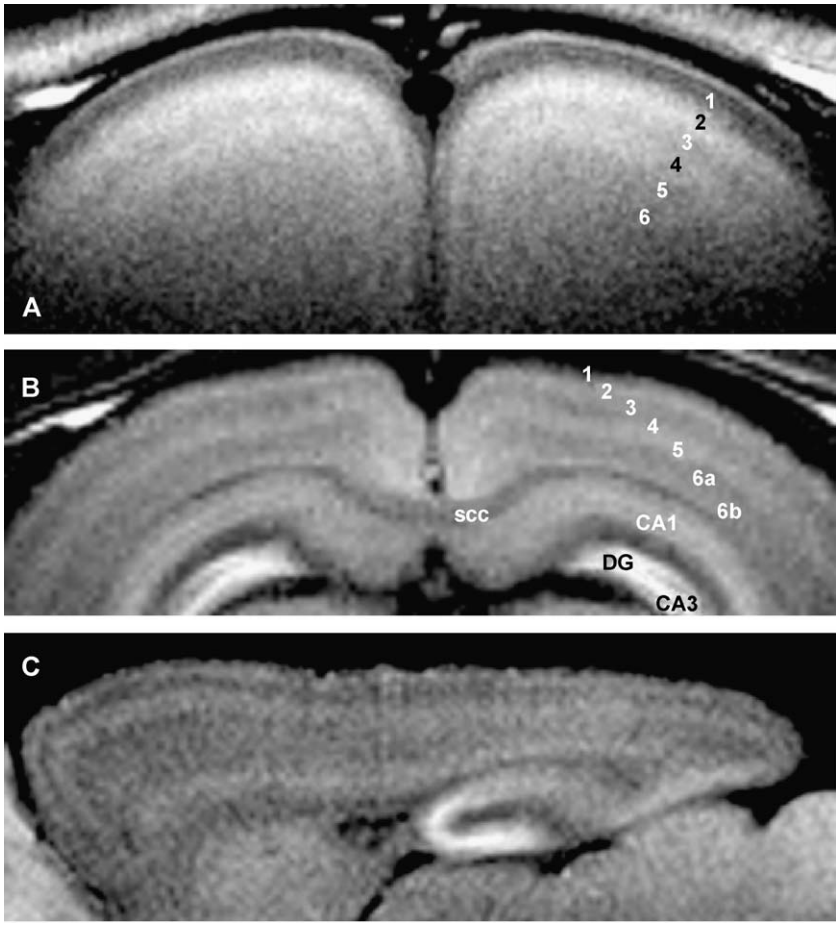

Fig. 8. Manganese-enhanced MRI of the layer structure of the cortex. Layer structure of the cortex detected by T_1-weighted MRI 4 days after administration of $MnCl_2$: (A) coronal slice in the frontal cortex using high spatial resolution (50 × 50 × 750 μm) and (B) coronal slice in occipital cortex (75 × 75 × 1000 μm), (C) sagittal slice (75 × 75 × 1000 μm) in same rat as B. Heterogeneous enhancement of T_1-weighted MRI was observed at least 1 day after administration of $MnCl_2$. A sagittal view showing layers running through the whole length of cortex is shown (C). The cell dense layers 2, the transition between layers 4 and 5 (4/5), and 6b enhanced more than the other layers 1 day after $MnCl_2$ administration. Layers 1, 3, and 6a enhanced much less. A deep thin layer of enhancement, assigned to layer 6b, could be detected (B). B and C were detected with inversion recovery and a spin-echo sequence.

layer showed statistically significant differences between each other although they are both highly enhanced. The normal control T_1-weighted image did not show statistically significant differences (Table 2B). The differentially enhanced layers could be detected throughout the OB (data not shown).

Cortex: Fig. 8 shows that there was heterogeneous enhancement of T_1-weighted MRI 1 day after administration of $MnCl_2$ in the cortex. The enhancement occurred in layers that could be detected throughout the cortex. Examples of MRI from a section in the frontal cortex (Fig. 8A) and the occipital cortex (Fig. 8B) are shown. A sagittal view showing layers running through the whole length of cortex is shown in Fig. 8C. No evidence of cortical layers could be detected in controls before having $MnCl_2$ administered. The cortex can be broken down into six major layers based on a variety of cell staining techniques in tissue sections. The layers were assigned based on the position of the enhanced layers compared to the Paxinos atlas (Paxinos and Watson, 1998; Paxinos et al., 1999). The transition between layers 2 and 3 (2/3), the transition between layers 4 and 5 (4/5) and 6b enhanced more than the other layers 1 day after $MnCl_2$ administration. Layers 1, 3, and 6a enhanced less. Indeed, it was difficult to distinguish layers 5 and 6 through most of the cortex. Each of the adjacent cortical layers between layers 1 and 5 showed significantly different relative signal as shown in Table 2C. T_1-weighted MRI of control brains that had not received $MnCl_2$ did not show any statistically significant differences in signal intensity in the cortex (data not shown).

Discussion

$MnCl_2$ administration leads to MRI contrast that represents neuronal architecture

The important finding of this work is that manganese-enhanced MRI enables contrast in living animals that defines neuroarchitecture. Many specific brain structures can be distinguished after $MnCl_2$ administration that are otherwise difficult to detect by MRI. These results are consistent with studies by other workers studying MRI enhancement in humans (Yamada et al., 1986), monkeys (Newland et al., 1989), and rodents (London et al., 1989) due to manganese exposure either to study the distribution of manganese in the brain or to begin to develop manganese as a useful brain MRI contrast agent (Aoki et al., 2002a; Lin, 1997; Watanabe et al., 2002). In addition, we have

demonstrated that within specific brain structures, there is contrast that reveals cytoarchitecture as evidenced by detection of the three layers consisting of the molecular, Purkinje, and granule cell layers in cerebellum, the granule cell layer in CA, six of eight layers in the OBs, and four of six cortical layers. This is the first in vivo whole-brain imaging technique that gives such anatomical detail nondestructively.

An interesting aspect of using manganese-enhanced MRI to study brain anatomy is that different structures enhance depending on the time after administration of $MnCl_2$. Very early (within 10 min) after administration of $MnCl_2$, the CP is specifically enhanced enabling MRI characterization of this important blood–CSF barrier. A bit later, the CSF is enhanced, which enables MRI definition of ventricles. Characterization of CSF is usually accomplished with T_2-weighted MRI; however, T_1 weighting may have advantages for faster data acquisition strategies. One day after administration of $MnCl_2$, there is heterogeneous but stereotypical enhancement of the brain. It is at this time point that the cytoarchitectural information available from manganese-enhanced MRI is strongest. In many brain areas, specific structures are clearly defined by administration of $MnCl_2$, which should make it possible to quantitatively follow volumes of these areas and the thickness of specific cell layers in a variety of animal models. The contrast is very high, which should make automatic segmentation of many brain areas feasible. The ability to rapidly assess sizes of a variety of brain areas by MRI should have an impact in analyzing the developmental changes in brain structure, changes in brains structure due to injury, and help analyze structural changes in the increasing number of interesting mouse mutants.

Comparison to previous work

The basic finding of differential MRI enhancement of specific brain regions after administration of Mn^{2+} is consistent with previous work. Below, comparisons are made region by region.

Choroid plexus, ventricle, circumventricular organs, and CSF: The early enhancement of ventricle, circumventricular organs, and CSF is consistent with earlier work in rodent that studied MRI enhancement after intraperitoneal administration of $MnCl_2$ (London et al., 1989). Here we have better defined the time course and show that CP enhances before CSF in the ventricles. This agrees with the observation that there is a fast transport system for Mn^{2+} into brain and the transport rate for CP is 100 times faster than other brain areas (Murphy et al., 1991; Rabin et al., 1993). After CSF, periventricular regions enhance primarily in ependymal layers around ventricles and the surface of cortex and OB. By 1 day after IV administration of $MnCl_2$, ventricles no longer show MRI enhancement consistent with the idea that the manganese is actively transported from CP to CSF and then to brain tissue. In a recent study that used intraperitoneal administration of $MnCl_2$ into the mouse, significant enhancement was detected in the CP up to 48 h after manganese administration (Watanabe et al., 2002). This is different than our finding in rat and may be due to the different route of administration or different dose of $MnCl_2$ used.

The rapid enhancement of circumventricular organs, such as Pit and Pi, is consistent with previous MRI work in the mouse that detected significant enhancement in these organs at 6 h (Lin, 1997; London et al., 1989; Watanabe et al., 2002). Here we show that the enhancement is very rapid, occurring within the first few minutes of infusion of $MnCl_2$. These areas do not have a BBB and this result argues that uptake into other brain regions is limited by the BBB as demonstrated when $MnCl_2$ was used over short time scales (10 min) to selectively enhance active regions of the brain (Lin and Koretsky, 1997).

Olfactory bulb: The large enhancements in the OB detected 24 h after intravenous administration of $MnCl_2$ are consistent with previous autoradiographic studies (Takeda et al., 1998a; Tjalve et al., 1996) and recent MRI studies of the rodent (Lin, 1997; Watanabe et al., 2002). Previous MRI studies of monkey and rat failed to detect enhancement in the OB probably due to the lower resolution obtained (London et al., 1989; Newland et al., 1989). Watanabe et al. (2002) observed four layers as alternating high and low signals and suggested that the high signals originated from the glomerular layer and the mitral cell layer. Here we delineated six layers of alternating signal intensity in the rat and assigned them based on comparison to the rat atlas. The glomerular layer and mitral cell layer are the most cell dense layers of the OB, which indicates that one possibility to explain differential enhancement due to $MnCl_2$ is that regions with high cell density are more enhanced (Royet et al., 1988; Shipley and Adamek, 1984). The early enhancement of the olfactory nerve layer and surface of the OB argues that most of the $MnCl_2$ in the bulb entered via CP and the subarachnoid space. It has been previously shown that significant MRI enhancement changes in the OB can be achieved by direct application of $MnCl_2$ to the nose (Pautler et al., 1998). This work showed that MRI could follow the movement of Mn^{2+} along nerve tracts leading to the use of manganese as a noninvasive tract tracer and demonstrated that manganese can enter the brain via peripheral nerves.

Hippocampus: The CA had a large degree of enhancement and specifically in the DG and Ammon's horn region of CA. That the CA can accumulate systemically administered $MnCl_2$ is consistent with previous autoradiographic studies (Takeda et al., 1994a, 1998b) and recent MRI work in the rodent (Lin, 1997; Watanabe et al., 2002). Earlier MRI work in rat and monkey did not detect enhancement in CA probably due to relatively low spatial resolution used (London et al., 1989; Newland et al., 1989). Here, greater enhancement was detected in granule cell layer and hilus of the DG than surrounding tissue and in the pyramidal cell layer of the hippocampal formation. Enhancement decreased from CA3 to CA1; however, the pyramidal cell layer decreases in thickness and the decreased enhancement may be due to partial volume effects in CA1 and CA2 at the resolutions used.

Cerebellum: Enhancement in the cerebellum detected here is consistent with previous findings by autoradiography (Takeda et al., 1998b; Valois and Webster, 1989) and MRI (Lin, 1997; Watanabe et al., 2002) in the rat and mouse. However, the present work is the first that shows a laminar structure with the enhanced molecular and granule cell layers segmented by the less-enhanced Purkinje cells.

Cortical areas: Enhancement in cortical areas at 24 h after $MnCl_2$ administration was less than that detected in OB, CA, and cerebellum. This is also consistent with previous autoradiography studies (Valois and Webster, 1989; Takeda et al., 1998b) and recent MRI studies (Lin, 1997; Watanabe et al., 2002) in the rat and mouse. One of the most interesting and unique aspects of the present study was that there was a clear layering of enhancement in the cortex. Comparison to the atlas led us to assign the layers with the greatest amount of enhancement to layers 2/3 and 4/5 in both frontal and occipital cortex. In addition, a small band of enhancement was detected deep in layer 6 in the occipital cortex, which may be due to layer 6b.

Mechanism of Mn uptake into brain

Manganese is a component of the mitochondrial form of superoxide dismutase (Sugaya et al., 1997), and is needed for glutamine synthetase activity in astrocytes (Carl et al., 1993). The largest subcellular manganese concentration is in the mitochondria, although in excess it also accumulates in lysosomes (Suzuki et al., 1983). The present results add some information to understanding the mechanism of uptake of manganese into the brain. IV administration of $MnCl_2$ to anesthetized rats leads to signal enhancement initially in CP and circumventricular organs that do not have BBB. In the CSF compartment, signal enhancement was extended from CP to ventricle and subarachnoid space, and also into the luminal linings of ventricular walls. The signal enhancement in CP was lost immediately after stopping the $MnCl_2$ infusion. These results are indicative that manganese ion, probably Mn^{2+}, can be uptaken and cross the blood–CSF barrier via CP. This agrees with the observation that there is a fast transport system for Mn^{2+} into brain and the transport rate for CP is 100 times faster than other brain areas (Murphy et al., 1991; Rabin et al., 1993). In addition to the CSF compartment, circumventricular organs, especially in Pit, also showed rapid increase in signal intensity. In all circumventricular organs except the subcommissural organ, the capillaries have fenestrated endothelial cells (Weindl and Joynt, 1973). Therefore, the BBB is disrupted in all but one of the circumventricular organs (Oldfield and McKinley, 1995; Weindl and Joynt, 1973). This agrees with the observation made by London et al. (1989) that IP manganese injection lead to high manganese accumulation in ventricles, Pi, and Pit in anesthetized rats.

As time progressed, high signal intensity appeared to slowly move out of the ventricular systems and redistribute into brain areas. All around the brain regions that are close to CSF such as the periventricular brain tissue (i.e., CP, fimbria of hippocampus, and dorsal and intermediate part of lateral septal nucleus), surface of cortex, and outer surface of OB enhanced 30–60 min after starting the manganese infusion. This result suggests that manganese is uptaken from CSF to brain tissues via ependyma surrounding ventricles. Within 2 h, the ventricular hyperintensity moved into the areas that surround the CSF compartments such as hypothalamus, OB, fimbria of hippocampus, ventral end of CA, ventral end of cerebellum, and the surface of cortex. In particular, enhancement of fimbria of hippocampus near lateral ventricle suggested that manganese uptake occurs via the choroid fissure and fimbria of hippocampus to DG and CA. After 1 day, signal enhancement reached its final pattern: CA, Pit, OB, cerebellum, and basal forebrain, which include basal ganglia and hypothalamus. It may be that the mechanism for movement of manganese from ependyma throughout the brain is similar to that which results in anterograde movement of manganese along appropriate neuronal pathways when applied intracerebrally or intraventricularly (Sloot and Gramsbergen, 1994; Takeda et al., 1994b). The relative distribution of enhancement did not change for the 2 weeks studied. There was just a slow loss of enhancement over 2 weeks. This agrees with previous data that intracranial manganese has an extremely slow clearance rate that can take up to 300 days (Lin, 1997; Newland et al., 1989).

While the bulk of the MRI enhancement detected in the brain is probably due to manganese that enters CSF through CP, there is evidence for other pathways. It has been demonstrated that manganese can enter the brain when applied to the nasal cavity (Pautler et al., 1998). Furthermore, the result that the surfaces of the OB and cortex were enhanced 2 h after manganese administration suggests the existence of another manganese pathway that is not via the choroids plexus. There is controversy about whether manganese can cross the BBB. Some evidence indicates that Mn^{2+} cannot cross the BBB (Kaur et al., 1980; Lin and Koretsky, 1997; Maynard and Cotzias, 1955). However, there is evidence that Mn^{2+} can cross the BBB (Aschner and Aschner, 1990, 1991; Aschner and Gannon, 1994; Dickinson et al., 1996; Kabata et al., 1989; Rabin et al., 1993). The present results are consistent with the notion that the ability of manganese to cross the BBB varies in different regions of the brain. Surface vessels around the OB and cortex may transport more manganese than vessels deeper in the brain.

Mechanisms for heterogeneous enhancements

The fact that manganese accumulation in the brain is heterogeneous is well appreciated and an active area of research with the aim of understanding the pathophysiology of movement disorders associated with high levels of manganese exposure. Some evidence suggests that most manganese is in astrocytes. Estimates range as high as 80% of the manganese in the brain is a functional component of glutamine synthetase (Wedler and Denman, 1984). In addition, evidence indicates that astrocytes are initial targets of manganese toxicity in the central nervous system after intranasal administration (Henriksson and Tjalve, 2000). Therefore, the distribution of manganese may relate to density of astrocytes. Evidence that manganese also accumulates in neurons comes from the fact that manganese will move in an anterograde direction along appropriate neuronal pathways and that increased activity due to pharmacological, odor, and somatosensory stimulation leads to rapid accumulation of manganese into the appropriate regions of the brain (Pautler and Koretsky, 2002; Pautler et al., 1998). These results suggest that manganese distribution in the brain may be dictated by neuronal cell density and/or activity. All of the regions that have high enhancement after 1 day are regions of high neuronal density and high activity including the OB, CA, and cerebellum. Indeed, the increased enhancement within subregions of these areas also correspond to cell dense and very active regions including the glomerular layer of the OB, the granular cell layer of the CA, and the granule cell layer of the cerebellum.

Manganese has been recognized to be a neurotoxin for over a century, leading to basal ganglia disorders such Parkinsonism and dystonia (Sloot and Gramsbergen, 1994). It is not clear in the present studies how much manganese gets to the brain to compare to concentrations known to be neurotoxic. In some animals, there was an acute reaction to the systemic $MnCl_2$, including loss of temperature regulation and sluggishness. These symptoms resolved after a few hours and then no behavioral dysfunction was detected. Manganese is highly concentrated in liver and kidney, and the acute effects were likely due to systemic effects not related to brain accumulation of manganese. It is possible to use lower doses of $MnCl_2$ (Watanabe et al., 2002); however, it is not clear whether all the neuroarchitecture can be detected at lower doses. Sloot and Gramsbergen (1994) showed that it took direct injections of 400 mM $MnCl_2$ or greater to cause significant changes in dopamine and disruption in Ca^{2+} metabolism took higher doses. Regional MRI contrast that we detect from the systemic administration used here is much lower than regional MRI contrast detected by direct injection of 10 mM $MnCl_2$ (data not shown), indicating that the amount of manganese that accumulates in the brain in below

neurotoxic levels. Future studies will quantify the amount of manganese getting to the brain and test for any neurotoxic effects.

Conclusions

There continues to be steady progress in increasing resolution with MRI techniques, thanks to increased magnetic field strengths and progress in MRI detector technologies. As resolutions approach histological levels in the intact animal, it is becoming increasingly important to develop techniques that enable interesting and relevant contrast at these resolutions. Here we demonstrate that a systemic dose of manganese is a useful brain contrast agent for defining brain regions (Aoki et al., 2002a; Lin, 1997). At high resolution, details of neuroarchitecture can be detected using manganese-enhanced MRI including layers in several brain regions including the cerebral cortex. This will enable noninvasive imaging of changes in these structures under a variety of conditions. Furthermore, the contrast is large enough that it may be able to automate segmentation and quantification of several brain regions. This holds the potential for making MRI a high-throughput technique to study changes in brain structure.

Acknowledgments

The authors thank Mr. Daryl Despres and Ms. Torri Wilson for assistance with animal preparation; Drs. Emmanuel L. Barbier and Florence Kernec for discussion; and Drs. Terri Clark and Judith A Davis (Animal Health and Care Section, National Institutes of Health, USA) for animal care advice. We also thank Dr. Chuzo Tanaka and Dr. Toshihiko Ebisu (Medical MR Center, Meiji University of Oriental Medicine, Japan) for helpful advice, Mr. Chia-Shan Hou, Dr. Masahiro Umeda, and Dr. Masaki Fukunaga for technical support of MRI measurement and analysis.

References

Aoki, I., Lin Wu, Y.J., Silva, A.C., Koretsky, A.P., 2002a. Cortical Layers Revealed by Manganese Enhanced Magnetic Resonance Imaging (MEMRI) in the Rat Brain after Systemic Administration. Proceedings of International Society for Magnetic Resonance in Medicine, Tenth Scientific Meeting and Exhibition. Honolulu, Hawaii, pp. 715.

Aoki, I., Tanaka, C., Takegami, T., Ebisu, T., Umeda, M., Fukunaga, M., Fukuda, K., Silva, A.C., Koretsky, A.P., Naruse, S., 2002b. Dynamic activity-induced manganese-dependent contrast magnetic resonance imaging (DAIM MRI). Magn. Reson. Med. 48, 927–933.

Archibald, F.S., Tyree, C., 1987. Manganese poisoning and the attack of trivalent manganese upon catecholamines. Arch. Biochem. Biophys. 256, 638–650.

Aschner, M., Aschner, J.L., 1990. Manganese transport across the blood–brain barrier: relationship to iron homeostasis. Brain Res. Bull. 24, 857–860.

Aschner, M., Aschner, J.L., 1991. Manganese neurotoxicity: cellular effects and blood–brain barrier transport. Neurosci. Biobehav. Rev. 15, 333–340.

Aschner, M., Gannon, M., 1994. Manganese (Mn) transport across the rat blood–brain barrier: saturable and transferrin-dependent transport mechanisms. Brain Res. Bull. 33, 345–349.

Bandettini, P.A., Wong, E.C., Hinks, R.S., Tikofsky, R.S., Hyde, J.S., 1992. Time course EPI of human brain function during task activation. Magn. Reson. Med. 25, 390–397.

Barbeau, A., 1984. Manganese and extrapyramidal disorders (a critical review and tribute to Dr. George C. Cotzias). Neurotoxicology 5, 13–35.

Barbier, E.L., Marrett, S., Danek, A., Vortmeyer, A., van Gelderen, P., Duyn, J., Bandettini, P., Grafman, J., Koretsky, A.P., 2002. Imaging cortical anatomy by high-resolution MR at 3.0T: detection of the stripe of Gennari in visual area 17. Magn. Reson. Med. 48, 735–738.

Brurok, H., Skoglund, T., Berg, K., Skarra, S., Karlsson, J.O., Jynge, P., 1999. Myocardial manganese elevation and proton relaxivity enhancement with manganese dipyridoxyl diphosphate. Ex vivo assessments in normally perfused and ischemic guinea pig hearts. NMR Biomed. 12, 364–372.

Carl, G.F., Blackwell, L.K., Barnett, F.C., Thompson, L.A., Rissinger, C.J., Olin, K.L., Critchfield, J.W., Keen, C.L., Gallagher, B.B., 1993. Manganese and epilepsy: brain glutamine synthetase and liver arginase activities in genetically epilepsy prone and chronically seizured rats. Epilepsia 34, 441–446.

Dickinson, T.K., Devenyi, A.G., Connor, J.R., 1996. Distribution of injected iron 59 and manganese 54 in hypotransferrinemic mice. J. Lab. Clin. Med. 128, 270–278.

Donaldson, J., 1987. The physiopathologic significance of manganese in brain: its relation to schizophrenia and neurodegenerative disorders. Neurotoxicology 8, 451–462.

Duong, T.Q., Silva, A.C., Lee, S.P., Kim, S.G., 2000. Functional MRI of calcium-dependent synaptic activity: cross correlation with CBF and BOLD measurements. Magn. Reson. Med. 43, 383–392.

Duong, T.Q., Kim, D.S., Ugurbil, K., Kim, S.G., 2001. Localized cerebral blood flow response at submillimeter columnar resolution. Proc. Natl. Acad. Sci. U. S. A. 98, 10904–10909.

Gorell, J.M., Johnson, C.C., Rybicki, B.A., Peterson, E.L., Kortsha, G.X., Brown, G.G., Richardson, R.J., 1997. Occupational exposures to metals as risk factors for Parkinson's disease. Neurology 48, 650–658.

Graham, D.G., 1984. Catecholamine toxicity: a proposal for the molecular pathogenesis of manganese neurotoxicity and Parkinson's disease. Neurotoxicology 5, 83–95.

Heimer, L., Zahm, D.S., Alheid, G.F., 1995. Basal ganglia. In: Paxinos, G. (Ed.), The Rat Nervous System, second ed. Academic Press, San Diego, pp. 579–628.

Henriksson, J., Tjalve, H., 2000. Manganese taken up into the CNS via the olfactory pathway in rats affects astrocytes. Toxicol. Sci. 55, 392–398.

Hu, T.C., Pautler, R.G., MacGowan, G.A., Koretsky, A.P., 2001. Manganese-enhanced MRI of mouse heart during changes in inotropy. Magn. Reson. Med. 46, 884–890.

Kabata, H., Matsuda, A., Yokoi, K., Kimura, M., Itokawa, Y., 1989. The effect of the dosage and route of manganese administration on manganese concentration in rat brain. Nippon Eiseigaku Zasshi 44, 667–672.

Kaur, G., Hasan, S.K., Srivastava, R.C., 1980. The distribution of manganese-54 in fetal, young and adult rats. Toxicol. Lett. 5, 423–426.

Kida, I., Xu, F., Shulman, R.G., Hyder, F., 2002. Mapping at glomerular resolution: fMRI of rat olfactory bulb. Magn. Reson. Med. 48, 570–576.

Koenig, S.H. , Brown III, R.D., Goldstein, E.J., Burnett, K.R., Wolf, G.L. 1985. Magnetic field dependence of proton relaxation rates in tissue with added Mn^{2+}: rabbit liver and kidney. Magn. Reson. Med. 2, 159–168.

Kwong, K.K., Belliveau, J.W., Chesler, D.A., Goldberg, I.E., Weisskoff, R.M., Poncelet, B.P., Kennedy, D.N., Hoppel, B.E., Cohen, M.S., Turner, R., et al., 1992. Dynamic magnetic resonance imaging of human brain activity during primary sensory stimulation. Proc. Natl. Acad. Sci. U. S. A. 89, 5675–5679.

Lauterbur, P.C., 1973. Image formation by induced local interactions: examples employing nuclear magnetic resonance. Nature 242, 190–191.

Lin, Y.J., 1997. MRI of the Rat and Mouse Brain after Systemic Administration of $MnCl_2$ Carnegie Mellon University, Pittsburgh. 149 pp.

Lin, Y.J., Koretsky, A.P., 1997. Manganese ion enhances T_1-weighted MRI during brain activation: an approach to direct imaging of brain function. Magn. Reson. Med. 38, 378–388.

London, R.E., Toney, G., Gabel, S.A., Funk, A., 1989. Magnetic resonance imaging studies of the brains of anesthetized rats treated with manganese chloride. Brain Res. Bull. 23, 229–235.

Maynard, L.S., Cotzias, G.C., 1955. The partition of manganese among organs and intracellular organelles of the rat. J. Biol. Chem. 214, 489–495.

Menon, R.S., Ogawa, S., Strupp, J.P., Ugurbil, K., 1997. Ocular dominance in human V1 demonstrated by functional magnetic resonance imaging. J. Neurophysiol. 77, 2780–2787.

Murphy, V.A., Rosenberg, J.M., Smith, Q.R., Rapoport, S.I., 1991. Elevation of brain manganese in calcium-deficient rats. Neurotoxicology 12, 255–263.

Natt, O., Watanabe, T., Boretius, S., Radulovic, J., Frahm, J., Michaelis, T., 2002. High-resolution 3D MRI of mouse brain reveals small cerebral structures in vivo. J. Neurosci. Methods 120, 203–209.

Newland, M.C., Ceckler, T.L., Kordower, J.H., Weiss, B., 1989. Visualizing manganese in the primate basal ganglia with magnetic resonance imaging. Exp. Neurol. 106, 251–258.

Ogawa, S., Tank, D.W., Menon, R., Ellermann, J.M., Kim, S.G., Merkle, H., Ugurbil, K., 1992. Intrinsic signal changes accompanying sensory stimulation: functional brain mapping with magnetic resonance imaging. Proc. Natl. Acad. Sci. U. S. A. 89, 5951–5955.

Oldfield, B.J., McKinley, M.J., 1995. Circumventricular organs. In: Paxinos, G. (Ed.), The Rat Nervous System, second ed. Academic Press, San Diego, pp. 391–403.

Pautler, R.G., Koretsky, A.P., 2002. Tracing odor-induced activation in the olfactory bulbs of mice using manganese-enhanced magnetic resonance imaging. NeuroImage 16, 441–448.

Pautler, R.G., Silva, A.C., Koretsky, A.P., 1998. In vivo neuronal tract tracing using manganese-enhanced magnetic resonance imaging. Magn. Reson. Med. 40, 740–748.

Paxinos, G., Watson, C., 1998. The Rat Brain in Stereotaxic Coordinates. Academic Press, San Diego.

Paxinos, G., Kus, L., Ashwell, K.W.S., Watson, C., 1999. Chemoarchitectonic Atlas of the Rat Forebrain. Academic Press, San Diego.

Plowchalk, D.R., Jordan, J.P., Thomford, P.J., Mattison, D.R., 1987. Effects of manganese (Mn^{++}) and iron (Fe^{+++}) on magnetic resonance imaging (MRI) characteristics of human placenta and amniotic fluid. Physiol. Chem. Phys. Med. NMR 19, 35–41.

Rabin, O., Hegedus, L., Bourre, J.M., Smith, Q.R., 1993. Rapid brain uptake of manganese(II) across the blood–brain barrier. J. Neurochem. 61, 509–517.

Royet, J.P., Souchier, C., Jourdan, F., Ploye, H., 1988. Morphometric study of the glomerular population in the mouse olfactory bulb: numerical density and size distribution along the rostrocaudal axis. J. Comp. Neurol. 270, 559–568.

Saleem, K.S., Pauls, J.M., Augath, M., Trinath, T., Prause, B.A., Hashikawa, T., Logothetis, N.K., 2002. Magnetic resonance imaging of neuronal connections in the macaque monkey. Neuron 34, 685–700.

Shipley, M.T., Adamek, G.D., 1984. The connections of the mouse olfactory bulb: a study using orthograde and retrograde transport of wheat germ agglutinin conjugated to horseradish peroxidase. Brain Res. Bull. 12, 669–688.

Silva, A.C., Koretsky, A.P., 2002. Laminar specificity of functional MRI onset times during somatosensory stimulation in rat. Proc. Natl. Acad. Sci. U. S. A. 99, 15182–15187.

Sloot, W.N., Gramsbergen, J.B., 1994. Axonal transport of manganese and its relevance to selective neurotoxicity in the rat basal ganglia. Brain Res. 657, 124–132.

Sugaya, K., Chouinard, M.L., McKinney, M., 1997. Induction of manganese superoxide dismutase in BV-2 microglial cells. NeuroReport 8, 3547–3551.

Suzuki, H., Wada, O., Inoue, K., Tosaka, H., Ono, T., 1983. Role of brain lysosomes in the development of manganese toxicity in mice. Toxicol. Appl. Pharmacol. 71, 422–429.

Takeda, A., Akiyama, T., Sawashita, J., Okada, S., 1994a. Brain uptake of trace metals, zinc and manganese, in rats. Brain Res. 640, 341–344.

Takeda, A., Sawashita, J., Okada, S., 1994b. Localization in rat brain of the trace metals, zinc and manganese, after intracerebroventricular injection. Brain Res. 658, 252–254.

Takeda, A., Kodama, Y., Ishiwatari, S., Okada, S., 1998a. Manganese transport in the neural circuit of rat CNS. Brain Res. Bull. 45, 149–152.

Takeda, A., Sawashita, J., Okada, S., 1998b. Manganese concentration in rat brain: manganese transport from the peripheral tissues. Neurosci. Lett. 242, 45–48.

Tjalve, H., Henriksson, J., Tallkvist, J., Larsson, B.S., Lindquist, N.G., 1996. Uptake of manganese and cadmium from the nasal mucosa into the central nervous system via olfactory pathways in rats. Pharmacol. Toxicol. 79, 347–356.

Valois, A.A., Webster, W.S., 1989. Retention and distribution of manganese in the mouse brain following acute exposure on postnatal day 0, 7, 14 or 42: an autoradiographic and gamma counting study. Toxicology 57, 315–328.

Van der Linden, A., Verhoye, M., Van Meir, V., Tindemans, I., Eens, M., Absil, P., Balthazart, J., 2002. In vivo manganese-enhanced magnetic resonance imaging reveals connections and functional properties of the songbird vocal control system. Neuroscience 112, 467–474.

Walters, N.B., Egan, G.F., Kril, J.J., Kean, M., Waley, P., Jenkinson, M., Watson, J.D., 2003. In vivo identification of human cortical areas using high-resolution MRI: an approach to cerebral structure–function correlation. Proc. Natl. Acad. Sci. U. S. A. 100, 2981–2986.

Wan, X.M., Fu, T.C., Smith, P.H., Brainard, J.R., London, R.E., 1991. Magnetic resonance imaging study of the rat cerebral ventricular system utilizing intracerebrally administered contrast agents. Magn. Reson. Med. 21, 97–106.

Wan, X., Fu, T.C., London, R.E., 1992. Charge dependence of the distribution of contrast agents in rat cerebral ventricles. Magn. Reson. Med. 27, 135–141.

Watanabe, T., Michaelis, T., Frahm, J., 2001. Mapping of retinal projections in the living rat using high-resolution 3D gradient-echo MRI with Mn^{2+}-induced contrast. Magn. Reson. Med. 46, 424–429.

Watanabe, T., Natt, O., Boretius, S., Frahm, J., Michaelis, T., 2002. In vivo 3D MRI staining of mouse brain after subcutaneous application of $MnCl_2$. Magn. Reson. Med. 48, 852–859.

Wedler, F.C., Denman, R.B., 1984. Glutamine synthetase: the major Mn(II) enzyme in mammalian brain. Curr. Top. Cell. Regul. 24, 153–169.

Weindl, A., Joynt, R.J., 1973. Barrier properties of the subcommissural organ. Arch. Neurol. 29, 16–22.

Wendland, M.F., Krombach, G.A., Higgins, C.B., Novikov, V., Saeed, M., 2002. Contrast enhanced MRI of stunned myocardium using Mn-based MRI contrast media. Acad. Radiol. 9 (Suppl. 2), S341–S342.

Yamada, M., Ohno, S., Okayasu, I., Okeda, R., Hatakeyama, S., Watanabe, H., Ushio, K., Tsukagoshi, H., 1986. Chronic manganese poisoning: a neuropathological study with determination of manganese distribution in the brain. Acta. Neuropathol. (Berlin) 70, 273–278.

Yang, X., Hyder, F., Shulman, R.G., 1996. Activation of single whisker barrel in rat brain localized by functional magnetic resonance imaging. Proc. Natl. Acad. Sci. U. S. A. 93, 475–478.